JOURNAL OF SOLID STATE CHEMISTRY **53**, 398–405 (1984)

The Oxygen Defect Perovskite $Ca_3Mn_{1.35}Fe_{1.65}O_{8.02}$: A Highly Frustrated Antiferromagnet

N. NGUYEN, Y. CALAGE, F. VARRET, AND G. FEREY

Laboratoire de Cristallographie, Chimie et Physique des Solides, L.A. 251, ISMRA-Université, 14032 Caen Cedex, France

AND V. CAIGNAERT, M. HERVIEU, AND B. RAVEAU

Groupe de Physique et Chimie du Solide (ERA 609 et 682), Faculté des Sciences, Université du Maine, Route de Laval, B41-72041 Le Mans Cedex, France

Received October 14, 1983; in revised form February 8, 1984

A new oxygen defect perovskite $Ca_3Mn_{1.35}Fe_{1.65}O_{8.02}$ has been isolated. It crystallizes in the orthorhombic system with the following parameters: $a \simeq a_p\sqrt{2}$; $b \simeq 3a_p$, and $c \simeq a_p\sqrt{2}$. X-Ray diffraction shows that it corresponds to the second member of the structural series $(AMO_3)_m(AMO_2\square)$ and thus consists of double perovskite layers separated by tetrahedral layers. This phase, related to the brownmillerite structure, differs from the latter, in that it exhibits oxygen defects in the perovskite layer and an excess of oxygen in the tetrahedral layer. These results are explained by the ability of Mn^{III} to adopt pyramidal coordination. Its magnetic properties have been investigated by susceptibility and magnetization measurements and Mössbauer spectroscopy in the temperature range 4–300 K. The dependence of the freezing temperature on the measuring technique (125 K with Mössbauer spectroscopy and 100 K from magnetization), the wide range of temperature where the freezing of the spins occurs, the sensitivity of χ on the cooling magnetic field and the drastic lowering of C_M characterize a highly frustrated behavior due to cationic disorder in the structure.

Introduction

The formation of anionic defects in the ABO_{3-x} perovskites is mainly governed by the ability of the B ions to adopt several coordinations. In this respect, copper, iron, and manganese are potential candidates. Highly oxygen-deficient perovskite layers characterized by octahedral, pyramidal, and square planar coordinations of copper have recently been observed in the compounds $La_3Ba_3Cu_6O_{14+y}$ (*1*), $La_{2-x}Sr_xCuO_{4-x/2+\delta}$ (*2*), and $La_{2-x}A_xCu_2O_{6-x/2+\delta}$ (*3*). A series of microphases $Ca_n(Fe, Ti)_nO_{3n-1}$ (*4, 5*) derived from the brownmillerite $Ca_2Fe_2O_5$ (*6*) in which Fe^{3+} takes simultaneously a tetrahedral and an octahedral coordination, have been isolated and characterized. The behavior of manganese is also remarkable in that, in the stoichiometric perovskite $CaMnO_3$ (*7*), Mn^{4+} adopts the octahedral coordination, whereas in the oxygen defect perovskite $Ca_2Mn_2O_5$ (*7, 8*), Mn^{3+} has, like copper, a pyramidal coordination. This structural difference between $Ca_2Fe_2O_5$ and $Ca_2Mn_2O_5$

0022-4596/84 $3.00

led us to think that the system $Ca_2Fe_2O_5$–"$CaMnO_{3-x}$" could yield new oxygen-deficient perovskites. Moreover, the compounds of this system could exhibit unusual magnetic properties due to the simultaneous presence of manganese and iron. This paper contains a study of the structure and of the magnetic properties of the oxygen defect perovskite $Ca_3Mn_{1.35}Fe_{1.65}O_{8.02}$.

Experimental

Synthesis. The oxide $Ca_3Mn_{1.35}Fe_{1.65}O_{8.02}$ was prepared from a powder mixture of MnO_2, Fe_2O_3, and $CaCO_3$ first heated at 900°C in air and then at 1100°C for 1 day. The specimen was finally quenched to room temperature.

Chemical analysis. The weight loss during the reaction was measured with Setaram microbalance in order to determine the oxygen content of the final product. The oxygen content was also determined by chemical analysis: the oxide was dissolved in a hydrochloric acid solution with an excess of titrated ferrous solution (Mohr salt): the excess of Fe^{2+} was then back-titrated with $K_2Cr_2O_7$. The oxygen content could thus be determined, assuming that iron is tervalent and manganese is bivalent in the presence of an excess of Fe^{2+}.

Crystallographic study. Owing to the small size of the crystals, the crystallographic study of this phase was carried out by X-ray powder diffractometry and electron diffraction. X-Ray powder data were registered with a Philips diffractometer using Cu$K\alpha$ radiation. Scattering factors of ionic species (*9*) corrected for anomalous scattering were used for calculations of intensities. Refinements were performed on intensities using a program previously described by Pham *et al.* (*10*). Electron diffraction micrographs were observed on microcrystals deposited on a carbon grid, using a Jeol 100 CX electron microscope.

Magnetic study. ^{57}Fe Mössbauer studies were performed by the classical technique in the temperature range 4–300 K. In the same range of temperature, magnetic measurements were realized with a Faraday balance for susceptibilities and with a vibrating sample magnetometer for magnetization. The corresponding values were measured with and without an applied field during the cooling of the sample.

Results and Discussion

The oxide $Ca_3Mn_{1.35}Fe_{1.65}O_{8.02}$ was obtained as a well crystallized black powder. The formulation of this oxide suggested that it corresponds to the member $m = 2$ of the family $(CaMO_3)_m \cdot (CaMO_2\square)$, derived from brownmillerite, in which double perovskite layers alternate with planes of tetrahedra. However, taking into account an experimental error of 0.01 oxygen atom per formula unit, a small deviation from the ideal formula $Ca_3Mn_{1.35}Fe_{1.65}O_8$ cannot be ruled out.

Structural study. The electron diffraction study was carried out on about 50 crystals of this composition. All of them were found to be well ordered and characterized by an orthorhombic symmetry. The systematic absent reflections, $hkO: h \neq 2n$ led to three possible space groups: *Pmma*, *Pm2a*, and $P2_1ma$. The X-ray powder diffractograms could be indexed in agreement with the electron diffraction results, in an orthorhombic cell where parameters are closely related to the "a_p" parameter of the perovskite:

$$a = 5.332(2)\ \text{Å} \simeq a_p\sqrt{2},$$
$$b = 11.13(4)\ \text{Å} \simeq 3a_p,$$
$$c = 5.455(2)\ \text{Å} \simeq a_p\sqrt{2}.$$

In order to confirm the structural model related to the brownmillerite, structure calculations were performed from X-ray powder data corresponding to 34 reflections, i.e., 67 *hkl*. The distribution of the metallic

TABLE I

STRUCTURAL DATA OF THE COMPOUND $Ca_3Mn_{1.35}Fe_{1.65}O_{8.02}$

		x	y	z	τ	B (Å^2)
Ca_1	2(c)	0.25	0.5	0.75	1	0.6
Ca_2	4(d)	0.24	0.183	0.70	0.5	0.6
Ca_2'	4(d)	0.24	0.834	0.70	0.5	0.6
Oc_1 (Mn, Fe)	4(d)	0.27	0.332	0.259	0.5	0.6
Oc_2 (Mn, Fe)	4(d)	0.25	0.665	0.255	0.5	0.6
Te (Mn, Fe)	4(d)	0.232	0.0	0.237	0.5	0.6
O_1	2(a)	0.0	0.329	0.0	1	3.5
O_1'	2(a)	0.0	0.665	0.0	1	3.5
O_2	2(b)	0.0	0.33	0.5	1	3.5
O_2'	2(b)	0.0	0.66	0.5	1	3.5
O_3	2(c)	0.25	0.50	0.25	0.7	3.5
O_4	2(c)	0.25	0.17	0.25	1	3.5
O_4'	2(c)	0.25	0.829	0.25	1	3.5
O_5	2(a)	0.0	0.010	0	1	3.5
O_5'	2(b)	0.0	0.01	0.5	0.30	3.5

ions could not be obtained from the X-ray diffraction results due to the similar scattering factors of manganese and iron. An overall *B* factor was assigned, respectively, to the metallic atoms and to the oxygen atoms, in order to limit the number of variable parameters. Refinements of the atomic positions and of the two thermal parameters were first carried out in the centrosymmetric space group *Pmma*. The discrepancy factor $R_I = \Sigma|I_c - I_0|/\Sigma I_0$ could not be reduced below 0.126.

The noncentrosymmetric space group *Pm*2*a*. was then studied. Refining successively the positions of the metallic atoms, of the oxygen atoms, and the two *B* factors led to a final discrepancy factor $R = 0.062$. The final atomic positions given in Table I show that Ca_1 is in an ideal position and that the manganese and the iron ions in the octahedral sites (Oc_1 and Oc_2) and those in tetrahedral sites (Te) are only slightly displaced from the ideal positions. The main displacements with respect to the ideal perovskite concern the Ca_2 and Ca_2' ions.

These results confirm that the structure of $Ca_3Mn_{1.35}Fe_{1.65}O_{8.02}$ is derived from that of brownmillerite, in that we can distinguish two types of layers: double perovskite layers in which the metallic atoms exhibit mainly the octahedral coordination, and a tetrahedral layer (Fig. 1). However, oxygen vacancies are also observed in the perovskite layers, since the occupancy factor of the O_3 site is only 0.7: this can be explained by the presence on these sites of Mn^{3+} which can adopt the pyramidal coordination. Moreover, the "tetrahedral" layer exhibits, in fact, an excess of oxygen with respect to the classical "brownmillerite layer," the occupancy factor of the oxygen sites O_5' being 0.30 instead of 0.0 as a result in this layer a part of the

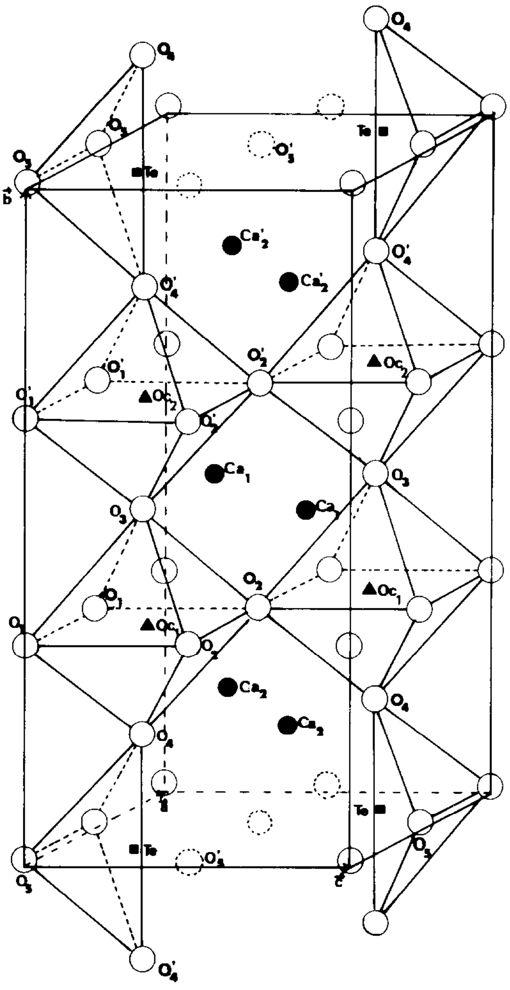

FIG. 1. Structure of $Ca_3Mn_{1.35}Fe_{1.65}O_{8.02}$.

TABLE II

INTERATOMIC DISTANCES FOR $Ca_3Mn_{1.35}Fe_{1.65}O_{8.02}$

Octahedron Oc_1–O		Octahedron OC_1 O–O		Tetrahedron Te O–O		Ca_2–O		Ca_2'–O	
Oc_1–O_1	2.017 Å	O_1–O_1	2.666 Å	O_4–O_5	2.605 × 2 Å	Ca_2–O_4	2.631 Å	Ca_2'–O_4'	2.456 Å
Oc_1–O_1	1.871	O_2–O_2	2.666	O_4–O_4'	3.795	Ca_2–O_4	2.460	Ca_2'–O_4'	3.001
Oc_1–O_2	1.950	O_1–O_2	2.728 × 2	O_5–O_4'	2.778 × 2	Ca_2–O_4	3.004	Ca_2'–O_4'	2.628
Oc_1–O_2	1.798	O_1–O_3	2.693 × 2	O_5–O_5	2.666	Ca_2–O_4	2.737	Ca_2'–O_4'	2.734
Oc_1–O_3	1.872	O_1–O_4	2.603 × 2	Ca_1–O		Ca_2–O_1	2.635	Ca_2'–O_1'	2.806
Oc_1–O_4	1.808	O_2–O_3	2.686 × 2			Ca_2–O_1	2.689	Ca_2'–O_1'	2.856
⟨Oc_1–O⟩	1.886	O_2–O_4	2.609 × 2			Ca_2–O_2	2.342	Ca_2'–O_2'	2.569
				Ca_1–O_3	2.728 × 2 Å	Ca_2–O_2	2.402	Ca_2'–O_2'	2.623
Octahedron Oc_2–O		Octahedron OC_2 O–O		Ca_1–O_3	2.666 × 2	Ca_2–O_5	2.832	Ca_2'–O_5	2.856
				Ca_1–O_2'	2.609 × 2	Ca_2–O_5	2.882	Ca_2'–O_5	2.905
Oc_2–O_1'	1.927 × 2 Å	O_1'–O_1'	2.666 Å	Ca_1–O_2	2.686 × 2	Ca_2–O_5'	2.561	Ca_2'–O_5'	2.578
Oc_2–O_2'	1.888 × 2	O_1'–O_4'	2.640 × 2	Ca_1–O_1	2.693 × 2	Ca_2–O_5'	2.615	Ca_2'–O_5'	2.632
Oc_2–O_3	1.837	O_1'–O_2'	2.728 × 2	Ca_1–O_1'	2.647 × 2				
Oc_2–O_4'	1.826	O_1'–O_3	2.647 × 2						
⟨Oc_2–O⟩	1.882	O_2'–O_2'	2.666						
Tetrahedron Te–O		O_2'–O_4'	2.679 × 2						
Te–O_4	1.896 Å	O_2'–O_3	2.609 × 2						
Te–O_4'	1.907								
Te–O_5	1.792								
Te–O_5	1.932								

metallic ions exhibit either the octahedral or the pyramidal coordination. It must also be emphasized that the Ca_2 and Ca_2' ions which are located at the boundary between the octahedral and the tetrahedral layers have more space owing to the absence of the oxygen of the tetrahedral layer, and are thus displaced one toward the other.

The interatomic distances are given in Table II. One of the octahedra Oc_1 is somewhat more distorted than the other Oc_2. The "height" of the tetrahedra is close to that of the octahedra, contrary to the brownmillerite, which exhibits more flattened tetrahedra. This feature could be due the presence of an excess of oxygen in the "tetrahedral layers," involving for the other metallic ions of this layer either a pyramidal or an octahedral coordination.

Mössbauer study. The room temperature spectrum (Fig. 2) shows that iron is present only in the tervalent state. Thus, the for-

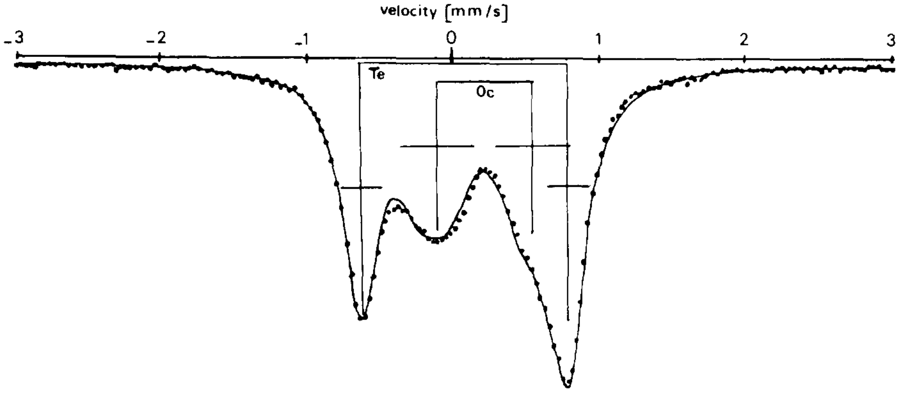

FIG. 2. Mössbauer resonance pattern of $Ca_3Mn_{1.35}Fe_{1.65}O_{8.02}$ at 293 K.

TABLE III

ROOM TEMPERATURE MÖSSBAUER DATA[a] OF $Ca_3Mn_{1.35}Fe_{1.65}O_{8.02}$

	Te sites	Oc sites	
δ	0.18(1)	0.33(2)	
Δ	1.41(1)	0.69(2)	$Fe^{III}_{Te}/Fe^{III}_{Te+Oc} = 0.48(5)$
Γ	0.26(2)[b]	0.50(4)[b]	

[a] Relative to iron metal at 300 K.

[b] The low precision is due to the overlap of the rays. δ: isomer shift (mm/sec). Δ: quadrupolar splitting (mm/sec).

mula of this oxide can be written $Ca_3Mn^{III}_{0.31}Mn^{IV}_{1.04}Fe^{III}_{1.65}O_{8.02}$. This pattern exhibits two paramagnetic contributions corresponding to tervalent iron in both octahedral and tetrahedral sites. For sake of simplicity, these sites will be noted Oc and Te, respectively. Table III gives the fitted experimental results at 293 K. Particularly for Oc sites, the results are in good agreement with previously given data which concern $Ca_2Fe_2O_5$ (*11–13*), $LaFeO_3$ (*14*), $Ca_2LaFe_3O_8$ (*15*), and $Ca_2Fe_{2-x}Ti_{2-2x}O_{6-x}$ (*16*). For both sites, the values of the isomer shifts and the very small temperature dependence of the quadruple splittings Δ ($\Delta_{300\,K}$ = 1.40 mm/sec, $\Delta_{150\,K}$ = 1.42 mm/sec) are consistent with a high spin behavior for iron(III).

Structurally, it was shown that the distortions of Oc_1 and Oc_2 octahedra were different (Table I). Moreover, it may be reasonably supposed that iron ions occupy these two octahedral sites. Thus, owing to the

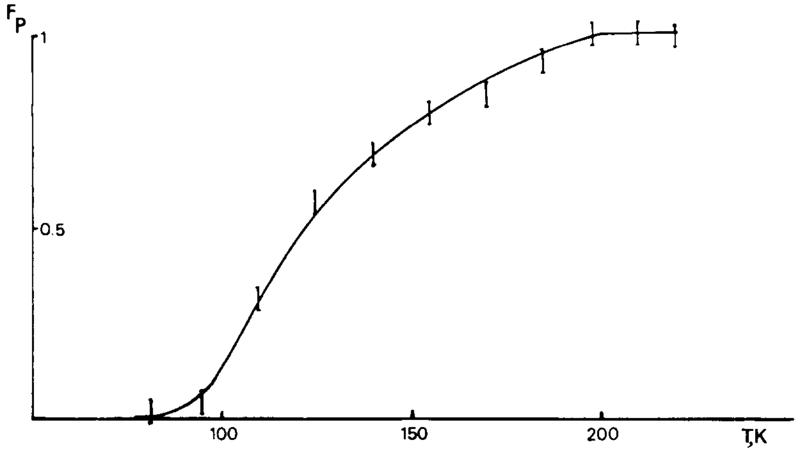

FIG. 3. Thermal variation of the paramagnetic fraction F_p of the compound $Ca_3Mn_{1.35}Fe_{1.65}O_{8.02}$.

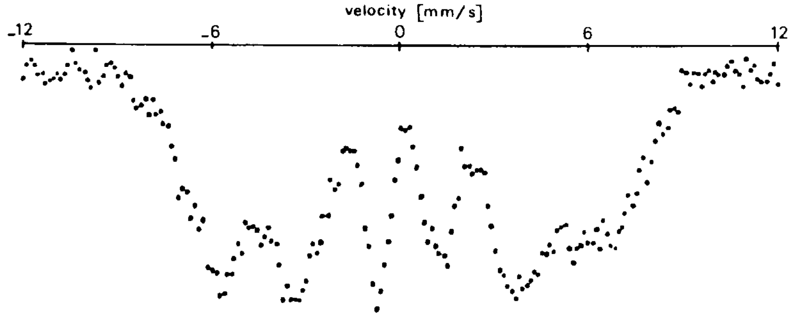

FIG. 4. Mössbauer resonance pattern of $Ca_3Mn_{1.35}Fe_{1.65}O_{8.02}$ at 77 K.

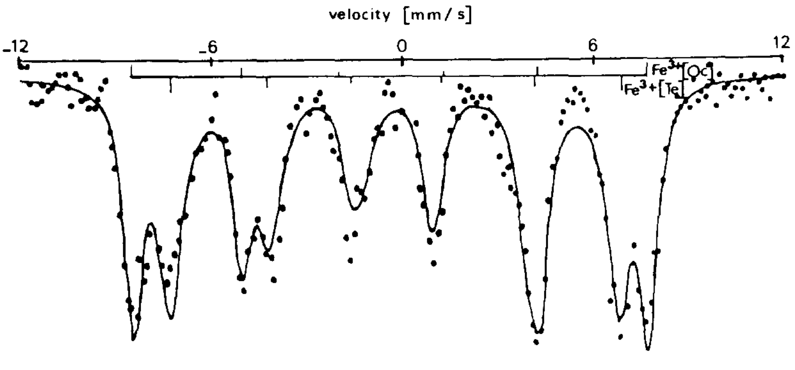

FIG. 5. Mössbauer resonance pattern of $Ca_3Mn_{1.35}Fe_{1.65}O_{8.02}$ at 4.2 K.

sensitivity of iron to its neighborhood, the Mössbauer characteristics of the two Oc sites must differ. Where the difference is too small to separate the two contributions, the spectra are fitted by only one mean contribution with a somewhat large width of the peak, related to the difference; this is the situation which occurs in this work. Consequently, the distribution of Fe^{3+} on Oc and Te sites was measured with a somewhat large error (~5%); it corresponds to 50 ± 5% of the Fe^{3+} ions in each site, and yields the formulation $Ca_3Mn^{III}_{0.31}Mn^{IV}_{1.04}(Fe^{III}_{Te})_{0.825}(Fe^{III}_{Oc})_{0.825}O_{8.02}$.

The Zeeman sextet begins to appear below 140 K. The magnetic transition was studied using both the "thermal scanning" technique (*17*) and by recording the whole spectra as a function of temperature. A drastic broadening of the lines is observed, while the paramagnetic doublet coexists with the Zeeman sextet in a remarkably wide range of temperature (100 K) as can be seen from the thermal variation of the paramagnetic fraction F_p (Fig. 3). The spectrum is still poorly resolved at 77 K (Fig. 4) far below the "average" magnetic ordering temperature, where the paramagnetic fraction F_p reaches 0.5 (125 K). At 4.2 K (Fig. 5), the hyperfine magnetic fields are significantly different: 438 kOe for Te sites and 504 kOe for Oc sites, in agreement with previous data (*18*).

Magnetization measurements. At every temperature, the variation of the magnetization σ as a function of the applied magnetic field is quasi-linear for zero-field cooled samples. Moreover, in the highest

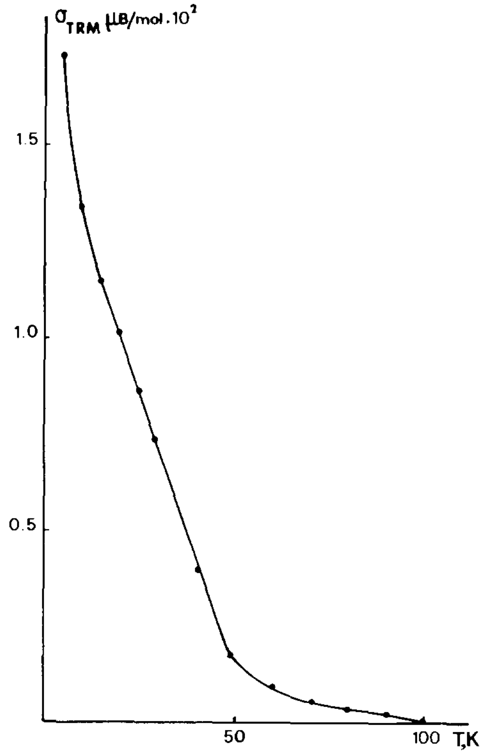

FIG. 6. Thermal variation of the thermoremanent magnetization (TRM) of the compound $Ca_3Mn_{1.35}Fe_{1.65}O_{8.02}$.

field of our experiments, σ reaches only 5% of the magnetization, which could be expected in the case of a ferromagnetic coupling. These two facts are sufficient to characterize the antiferromagnetic coupling of the spins. However, if the sample is cooled from 300 to 4.2 K when applying an external magnetic field (H = 18.8 kOe), the magnetization is enhanced by 15% and a remanent ferromagnetic component is observed, which did not exist when the sample was cooled without external field. The existence of such a thermoremanent magnetization (TRM) is typical of the misalignment of the spins in the magnetic structure (*21*). The freezing temperature of the spins using this technique (T_f = 100 K) corresponds to the cancellation of this TRM by increasing the temperature (Fig. 6).

Susceptibility measurements. They corroborate the above results (Fig. 7). Above 100 K, the Curie–Weiss law is well obeyed. The extrapolated θ_p value (−70 ± 5 K) agrees with the antiferromagnetic coupling of the spins, deduced from magnetization measurements. However, it must be noted that the experimental molar Curie constant $C_M = 6.03$ (*12*) is drastically lower than its theoretical value (10.09) calculated with all ions in a high spin state. It has been previously shown (*20*) that this feature corresponds to a wide spread of the exchange interactions.

Below T_f, the inverse susceptibility slightly increases when the sample is cooled without an external magnetic field, but its value depends on the measuring field, mostly at low fields (Fig. 7). On this figure, we also plotted χ^{-1} (T) when an external field is applied during the cooling of the sample: the curve decreases monotonically, without any change in the slope. As

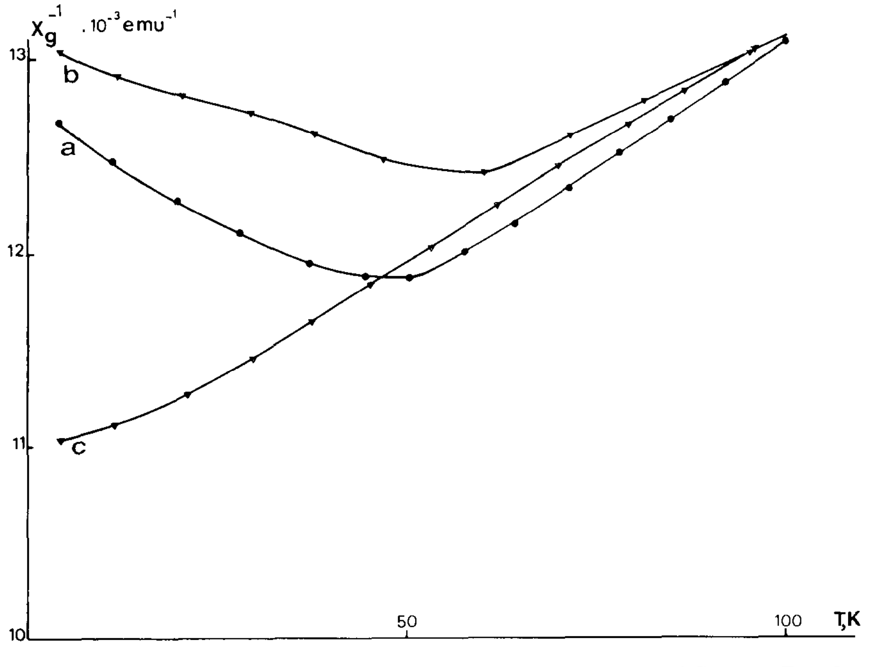

FIG. 7. Inverse susceptibility as a function of temperature of the compound $Ca_3Mn_{1.35}Fe_{1.65}O_{8.02}$. (a) Zero field cooled; measuring mean field 1500 Oe. (b) Zero field cooled; measuring mean field 8000 Oe. (c) Cooled and measured in a field H = 8000 Oe.

previously described (*20, 21*) this irreversible susceptibility confirms the misalignment of the spins, as already noted.

Discussion

Four main experimental features characterize the magnetic behavior of this compound:

(i) The large discrepancy between the value of T_f deduced from Mössbauer and magnetization data (*19*).

(ii) The wide range of temperature where magnetic freezing occurs progressively (100 K).

(iii) The significant dependence of the susceptibility on the cooling magnetic field (*20, 21*).

(iv) The drastic lowering of C_M, indicative of a wide spread in the exchange interactions, which are characteristic of antiferromagnetic amorphous insulating compounds.

This behavior is characteristic of speromagnetism (*20, 21*) which describes an isotropic freezing of the spins. It seems however unrealistic to imagine such an extreme situation for this crystalline compound, but the results are consistent with a distribution of the directions of the spins, and indicate an important frustration of the interactions (*22*). The topology of the metallic sublattice, which can be described from square platelets, cannot be responsible of this behavior. The magnetic interactions, deduced from Kanamori–Goodenough rules (*23, 24*), are mainly antiferromagnetic in nature but may be also ferromagnetic for Mn^{3+}–Mn^{4+} coupling. It is suggested that these competing interactions, combined with the cationic disorder as evidenced in the structural study, are responsible of the highly frustrated magnetic character of this compound.

References

1. J. Provost, F. Studer, C. Michel, and B. Raveau, *Synth. Met.* **4,** 147 (1981).

2. N. Nguyen, J. Choisnet, M. Hervieu, and B. Raveau, *J. Solid State Chem.* **39,** 120 (1981).

3. N. Nguyen, L. Er-Rakho, C. Michel, J. Choisnet, and B. Raveau, *Mater. Res. Bull.* **15,** 891 (1980).

4. J. C. Grenier, G. Schiffmacher, P. Caro, M. Pouchard, and P. Hagenmuller, *J. Solid State Chem.* **20,** 365 (1977).

5. J. C. Grenier, F. Ménil, M. Pouchard, and P. Hagenmuller, *Mater. Res. Bull.* **13,** 329 (1978).

6. E. F. Bertaut, P. Blum, and A. Sagnières, *Acta Crystallogr.* **12,** 149 (1959).

7. K. R. Poeppelmeier, M. E. Leonowicz, J. C. Scanlon, J. M. Longo, and W. B. Yelon, *J. Solid State Chem.* **45,** 71 (1982).

8. K. R. Poeppelmeier, M. E. Leonowicz, and J. M. Longo, *J. Solid State Chem.* **44,** 89 (1982).

9. D. T. Cromer and J. T. Waber, *Acta Crystallogr.* **18,** 104 (1965).

10. C. C. Pham, J. Choisnet, and B. Raveau, *Bull. Acad. R. Belg. Sci.* **61,** 473 (1975).

11. F. Pobell and F. Wittmann, *Phys. Lett.* **19,** 175 (1965).

12. R. W. Grant, H. Wiedersich, S. Geller, U. Gonser, and G. P. Espinosa, *J. Appl. Phys.* **38,** 1455 (1967).

13. J. C. Grenier, F. Ménil, M. Pouchard, and P. Hagenmuller, *C.R. Acad. Sci.* **277,** 647 (1973).

14. C. Boekema, F. Van der Woude, and G. A. Sawatzky, *Int. J. Magn.* **3,** 341 (1972).

15. J. C. Grenier, F. Ménil, M. Pouchard, and P. Hagenmuller, *Mater. Res. Bull.* **12,** 79 (1977).

16. J. C. Grenier, F. Ménil, M. Pouchard, and P. Hagenmuller, *Mater. Res. Bull.* **13,** 329 (1978).

17. G. Ferey, thèse de Doctorat d'Etat, Paris VI (1977).

18. N. N. Greenwood and T. C. Gibb, "Mössbauer Spectroscopy," p. 258, Chapman & Hall, London (1971).

19. A. Murani, *J. Appl. Phys.* **49,** 1604 (1978).

20. G. Ferey, F. Varret, and M. Coey, *J. Phys. C* **12,** 531 (1979).

21. G. Ferey, *Rev. Phys. Appl.* **15**(6), 1043 (1980).

22. G. Toulouse, *Commun. Phys.* **2,** 115 (1977).

23. J. Kanamori, *J. Phys. Chem. Solids* **10,** 87 (1959).

24. J. B. Goodenough, "Magnetism and the Chemical Bond," Interscience, New York (1963).